Abstract: (130 words)

Ventilation and dissolved oxygen in Lake Superior are key factors that determine the fate of various natural and anthropogenic inputs to the lake. We employ an idealized age tracer and biogeochemical tracers in a realistically configured numerical model of Lake Superior to characterize its ventilation and dissolved O_2 cycle. Our results indicate that Lake Superior is preferentially ventilated over rough bathymetry and that spring overturning following a very cold winter does not completely ventilate the lake interior. While this is unexpected for a dimictic lake, no part of the lake remains isolated from the atmosphere for more than 300 days. Our results also show that Lake Superior's oxygen cycle is dominated by solubility changes; as a result, the expected relationship between biological consumption of dissolved O_2 and ventilation age does not manifest.

Keywords: Lake Superior, numerical model, ventilation, ideal tracers, oxygen

1. Introduction

The "age" of a water parcel in the interior of a large water body is the time elapsed since that parcel was last exposed to the atmosphere and thus "ventilated." The maximum age of a water body can be considered its timescale of ventilation. This timescale is not the same as the residence time or the replacement time of water, which is about 180 years for Lake Superior [*Bennett*, 1978; *Matheson and Munawar*, 1978]. Even with no replacement (i.e., infinite residence time), there would be finite ventilation time as circulation transports surface waters into the interior. During ventilation, the surface waters exchange heat, water, and gases with the overlying atmosphere. At the same time, photosynthesis and other biological processes modify surface nutrient concentrations. These processes thus imprint signatures on the surface waters in terms of temperature, nutrients, and dissolved gas concentration, as well as salinity in the case of oceans. After being subducted, surface waters carry these signatures into the interior. If conservative, these initial or "preformed" signatures are preserved, save mixing, and serve as a unique tag of the location and conditions of the surface from which the water came.

Typically, a well-ventilated body of water has abundant dissolved oxygen (O_2). If the surface water were assumed to be in equilibrium with the overlying atmosphere, ventilation would initially carry saturation concentrations of dissolved O_2 from the surface into the interior. With time the O_2 concentration in the interior will be reduced, as aerobic respiration of organic matter consumes O_2. Thus, in chemical oceanography, this dissolved O_2 reduction can be considered a qualitative measure of ventilation.

Here we are interested in the ventilation timescale and the dissolved O_2 of Lake Superior, the largest lake in the world by surface area (82,100 km^2) with the mean depth of 147 m and maximum depth of 406 m. For its size, Superior has a relatively small watershed (127,700 km^2), located within the Canadian Shield, whose igneous and metamorphic rocks are strongly resistant to weathering. The allochthonous loading of dissolved constituents including nutrients is thus limited. As a result, the lake is oligotrophic and its organic carbon cycle is dominated by microbes [*Cotner et al.*, 2004]. The ventilation timescale, a fundamental physical characteristic of water bodies, is a key determinant of the fate of various natural and anthropogenic inputs to those bodies. For example, if the timescale were very short, any input will be quickly distributed throughout the water column and widespread in the surface sediments. In a coastal setting, relatively slow ventilation compared to the flux of nutrient delivery can cause widespread anoxia; a prominent example of this is the dead zone in the Gulf of Mexico near the mouth of the Mississippi River. Dissolved O_2 is also an important determinant of the fate of inputs, because oxidation facilitates degradation of many compounds, especially organic matter. In Lake Superior, the high dissolved O_2 at the lake bottom is expected to affect both the nitrogen cycle by limiting denitrification [*Small et al.*, 2014] and phosphorus cycle by increasing phosphorus retention [*Hecky*, 2000].

At the present time, very little is known about Lake Superior's ventilation or interior circulation in general. Of the great lakes, Lake Baikal has been studied perhaps most intensively in terms of deep water renewal. Baikal is located in a Siberian rift valley and thus very deep, reaching well in excess of 1500 m in the central basin. Mid-latitude lakes are typically dimictic; they overturn completely every spring and fall as the temperature of the surface water passes 4°C, the

temperature of maximum density of freshwater. However, this notion does not apply to very deep lakes due to the effect of pressure on the temperature of maximum density. For this reason, seasonal convective mixing is said to only reach down to depths of 250-350 m in Baikal [*Weiss et al.*, 1991; *Hohmann et al.*, 1997; *Schmidt et al.*, 2008]. Despite this thermobaric barrier, elevated concentrations of dissolved O_2 and CFCs are found at the bottom of Baikal and clearly indicate rapid ventilation [*Weiss et al.*, 1991]. Indeed, calculations of deep water renewal using helium and tritium data indicate that the renewal time is 10-18 years [*Hohmann et al.*, 1998]. Different mechanisms have been called upon to break the thermobaric barrier in Baikal: entry of slightly saline tributary water [*Hohmann et al.*, 1997], seasonal winds [*Weiss et al.*, 1991; *Schmidt et al.*, 2008], and cabbeling during the formation of spring time thermal bars [*Shimaraev et al.*, 1993].

In Lake Lucerne, Switzerland, seasonal winds and salinity from a tributary have been identified as triggers of deep water mixing [*Aeschlback-Hertig et al.*, 1996]. In Lake Issyk-Kul in central Asia, wintertime cooling appears to be the driver of rapid ventilation [*Peeters et al.*, 2003], which is indicated by measurements of anthropogenic tracers [*Hofer et al.*, 2002]. Wintertime cooling also appears to trigger cascading plumes of water in Lake Geneva [*Fer et al.*, 2002].

These studies of Baikal and other lakes indicate, perhaps not surprisingly, that key mechanisms of interior ventilation are different for different lakes. Key mechanisms are dependent, for example, on the depth of the lake, the prevailing atmospheric conditions, their seasonality, the presence of tributaries, and the catchment basins from which solutes are derived.

More relevant for Lake Superior is a study on tritium-helium age determination in Lakes Erie, Huron, and Ontario [*Torgersen et al.*, 1977]. Measurements on water samples collected over a summer yielded older ages for deeper lakes. The greatest maximum age was nearly 160 days (~6 months) in Lake Ontario, the deepest of the three lakes. This shows that the timescale of ventilation is months, not years, which is expected in dimictic lakes.

Lake Superior is dimictic. As noted, the thermobaric barrier to seasonal convective mixing occurs much deeper in Lake Baikal than the average depth of Superior, so the role of thermobaricity in the ventilation of Superior is likely not as important. An early modeling work has suggested that the time scale of horizontal mixing in Superior's hypolimnion, as well as in the epilimnion, is 2-3 years [*Lam*, 1978]. Other studies of circulation in Lake Superior, starting with an early report on the bottle drift experiment [*Harrington*, 1895], have also been primarily horizontal [*Beletsky et al.*, 1999; *Chen et al.*, 2001, 2002; *Bennington et al.*, 2010]. To our knowledge there is no study on the vertical mixing and therefore ventilation.

In terms of what is known about dissolved O_2 in Lake Superior, some data from the nearshore have been used to estimate respiration rates [*McManus et al.*, 2003; *Russ et al.*, 2004]. However, adequate spatial coverage is lacking, especially in the deeper, offshore waters. As a result, nearshore respiration rates have been extrapolated to the entire lake to determine its overall carbon budget. The lake-wide respiration rates thus estimated have typically been much higher than estimated production rates, leading to a conclusion that Lake Superior requires a significant amount of allochthonous carbon to close its carbon budget [*Cotner et al.*, 2004; *Urban et al.*, 2005]. A recent numerical model study suggests, however, that the nearshore respiration rates are

up to two orders of magnitude higher than offshore and that the extrapolation of nearshore rates to the entire lake is not justified [*Bennington et al.*, 2012]. The annual cycle of dissolved O_2 in Superior is not well documented.

We are motivated to fill these gaps in knowledge regarding Lake Superior's ventilation and dissolved O_2 cycle. We suspect that some waters of Lake Superior, especially in the deepest and bathymetrically complex parts (Figure 1), may in fact be significantly older and more oxygen depleted than expected from dimictic overturning. This suspicion is hinted by the oceanographic literature, which indicates that bathymetry constricts flow. For example, early radiocarbon data show that the eastern basin of the Atlantic Ocean is not as well-ventilated as the western basin [*Schlitzer*, 1986]. Separated by the mid-ocean ridge, the two Atlantic basins communicate by limited flow of deep and bottom waters through the Romanche, Vema Channel, and Chain Fracture Zones, as determined by temperature and salinity, nutrients [*Broecker and Peng*, 1982], chlorofluoromethanes [*Messias et al.*, 1999], and chlorofluorocarbon [*Rhein et al.*, 1998]. More generally, the global distribution of radiocarbon shows that the ventilation of the world ocean is dependent on the path of the deep and bottom waters [*Matsumoto*, 2007].

Another reason to suspect that Lake Superior's ventilation timescale may be longer than several months is that the spring and fall overturning does not imply that top-to-bottom convection occur everywhere at the same time. It is well known from early work by *Forel* [1880] that seasonal warming and cooling typically start from the periphery of the lake and work towards the center over days and weeks. The lateral temperature gradient associated with this seasonal warming and cooling is called the thermal bar, and has been observed in Lake Superior [*Hubbard and Spain*,

1973]. Remote sensing has captured it in all Laurentian Great Lakes [*Ullman et al.*, 1998]. During the thermal bar migration, lateral mixing and localized entrainment could facilitate large scale warming and cooling, even in the absence of lake-wide convection. Also, since Lake Superior has a large amount of thermal inertia, its deep water is typically close to 4°C year around. These reasons suggest that extensive convection may not be necessary for the entire lake to reach 4°C during each overturning with implications for the supply of dissolved O_2 into the interior.

Here we use a realistically configured numerical model of Lake Superior to characterize its ventilation and dissolved O_2 cycle. Following the seminal work of *England* [1995], we employ an idealized passive tracer *Age* to determine the ventilation time scale. At the same time, we simulate biogeochemical tracers using a simple ecosystem model to characterize the dissolved O_2 cycle. By simulating the distributions of these tracers under realistic meteorological conditions, we show that the ventilation of Lake Superior is significantly affected by the severity of winter conditions and that some parts of the lake may remain isolated from the surface for nearly a year. We also show that the expected relationship between biological consumption of dissolved O_2 and ventilation does not manifest, because the lake is so strongly dominated by physical processes.

2. Numerical Model and Experimental Design

The 3D numerical model of Lake Superior used in this study is based on an earlier version of our model [*White et al.*, 2012]. In the earlier version, we had developed the necessary atmospheric forcing fields by interpolating existing meteorological data from the NOAA National Buoy

Center array of open-lake buoys and Coastal Marine Automated Network stations. The new version of the model is forced by the North American Regional Reanalysis (NARR) output from National Center for Environmental Protection. The high resolution, gridded NARR output is available from 1979 to the present. For our model, we use NARR's surface radiative fluxes, wind, air temperature, pressure, humidity, and precipitation.

2.1 Physical Model

Our model is based on the Regional Ocean Modeling System (ROMS) [*Shchepetkin and McWilliams*, 2005], using the realistic bathymetric and coastal boundaries of Lake Superior of *White et al.* [2012]. The model simulates the hydrodynamics of Lake Superior with 20 terrain-following vertical levels, with vertical resolution less than one meter near the surface to about 50 meters at depth. The horizontal resolution is five kilometers in all directions. The model treats the lake as a closed basin without riverine input or output. Salinity is set to zero, and a freshwater equation of state is used [*Chen and Millero*, 1986].

The model has a dynamic and thermodynamic model of lake ice, which is critical for simulating a reasonable seasonal cycle of the temperature and density structure of Superior. To our knowledge this is the only model of Superior that has prognostic lake ice.

In the description of our earlier model [*White et al.*, 2012], simulated results for the period 1985-2008 were validated against observational data that included: time series of surface lake temperatures from the NOAA buoys; remotely sensed ice cover and surface temperatures; and depth profiles of temperature and chlorophyll from 19 offshore stations from the biannual EPA

surveys conducted in the early spring and late summer. Results from this model, now forced with NARR output, are superior to our earlier version of the model in most metrics we have examined and compare quite well with mean surface lake temperatures and mean daily ice coverage derived from satellite data (see Supporting Information). However, none of these observations can directly constrain the rate of interior circulation. Geochemical measurements like the tritium-helium age in Lakes Erie, Huron, and Ontario [*Torgersen et al.*, 1977] are not available in Lake Superior. Nevertheless, we assume that vertical mixing in our model is reasonably well simulated, because the earlier model results already compared favorably to the observed depth profiles of interior temperature and chlorophyll [*White and Matsumoto*, 2012], which are significantly controlled by vertical mixing. A good model-data agreement in surface ice cover [*White et al.*, 2012; Supporting Information] also suggests that vertical mixing in the model is reasonable, because the supply of heat by vertical mixing from below helps melt ice as does surface heat flux from the atmosphere. In addition, results from this model have been useful in informing the presence of remotely-sensed eddies in Lake Superior [*McKinney et al.*, 2012].

We note that *Bennington et al.* [2010] also use the NARR forcing to drive their model of Lake Superior, based on the MITgcm model architecture. They discuss the possibility of a warm bias in the NARR forcing (see Supporting Information).

2.2 Ecosystem Model

We follow the *White et al.* [2012] application of a NPZD-type ecosystem model [*Fasham et al.*, 1990], which uses phosphate as the limiting nutrient variable. Other important variables include chlorophyll, phytoplankton, zooplankton, and detritus. Overall the results of the biological model

are largely consistent with observed chlorophyll distribution [*White and Matsumoto*, 2012] and recent estimates of annual gross primary productivity (~5-10 Tg-C yr^{-1}) [*Cotner et al.*, 2004; *Urban et al.*, 2005; *Sterner, R.W.*, 2010, p.201].

The dissolved O_2 concentration is explicitly calculated in our model. The concentration at the surface is determined by air-lake exchange of O_2, which is driven by the gradient of pO_2 across the air-lake interface, solubility, and wind speed dependent gas exchange kinetics. If the residence time of surface water is comparable to the time scale of gas equilibration, which for O_2 is a few weeks in the ocean, the surface water will be nearly saturated. Away from the surface, the dissolved O_2 concentration will be reduced as organic matter is respired and nutrients are remineralized. This O_2 reduction, when quantified relative to the saturation concentration, is the apparent O_2 utilization (AOU). As water parcels become older, their dissolved O_2 is increasingly respired, thereby increasing AOU.

2.3 Idealized Tracer *Age*

Initially, the tracer *Age* is set everywhere to zero and transported passively. In the absence of ice, the time evolution of *Age* is illustrated in Figure 2 and governed by:

$$Age(\mathrm{x},\mathrm{y},\mathrm{z},\mathrm{t}) = \begin{cases} 0, & \mathrm{z} = 0 \\ Age(\mathrm{x},\mathrm{y},\mathrm{z},\mathrm{t}\text{-}1) + \Gamma\{Age(\mathrm{x},\mathrm{y},\mathrm{z},\mathrm{t})\} + \Delta\mathrm{t}, & \mathrm{z} > 0 \end{cases}, \qquad (1)$$

where tracer mixing by advection and diffusion is denoted by the transport operator Γ. The surface *Age* is continuously reset to zero throughout the simulations (i.e., being ventilated), except when there is ice. If a grid has 100% ice cover, which is rare in both the model and observation, ventilation is completely snuffed out and the surface water ages. With partial ice in a grid, there is partial ventilation; resetting of *Age* is proportional to the fraction of non-ice

coverage. Accounting for this ice effect has almost no impact on the lake-wide distribution of *Age* though, because even high ice concentration grid points typically have some leads, which allow fairly efficient *Age* resetting after some number of time steps. As soon as a parcel of water leaves the surface and becomes isolated from the atmosphere, the clock begins to tick, and tracer *Age* is incremented by Δt each time step (Figure 2b). Under steady state, the age of any grid box within the model domain would eventually achieve an equilibrium, whereby aging is balanced by the transport of younger, more ventilated waters. However, with episodic mixing such as convective overturning, *Age* in the interior can become younger quickly and even approach zero (Figure 2c). *Age* of a water parcel thus represents the weighted average time for the surface waters to reach the interior, so that a poorly ventilated interior grid box will have a high value. Waters near the surface will be younger in age, as the fractional contribution from surface waters will be larger. If the entire lake were ventilated within a short time period, *Age* everywhere would approach zero.

We have also simulated another, complementary, idealized tracer *Dye* [*England*, 1995]. The results of *Age* and *Dye* are entirely consistent in this study. The description and results of tracer *Dye* are presented as Supporting Information.

2.4 Experiments

Here we present results from simulations of the Lake Superior model spanning the calendar years 1997 and 1998. According to NOAA Great Lake Ice Atlas [*Assel*, 2003], winter ice coverage was extensive in 1997 and minimal in 1998. Our model is able to capture the large contrast in ice coverage (Figure 3). Also, we show that our model is able to simulate the seasonal changes in ice

coverage quite well (Supporting Information). Winter ice in Lake Superior has significant effects on the onset and duration of the subsequent summer stratified period. During stratification, there is no convective overturning and very limited ventilation.

The distributions of our idealized and biogeochemical tracers for 1997-1998 are thus expected to span the range of tracer distributions for years with both little and extreme ice coverage. This helps identify robust model behavior that is independent of the choice of meteorological forcing of the model and thus the severity of the seasonal variability. We note that while we only present results from the period 1997 and 1998, we also completed simulations for periods 1985-1987 (1985=significant ice year, 1987=ice minimum year) and 2006-2008 (2006=ice minimum year, 2008=significant ice year). The extent of the winter ice was well correlated with the ventilation time scale in all these simulation periods.

The model is spun up from a uniform state starting with 1994 meteorological forcing. It is run for an additional 2 years (1995-1996), which eliminates any effects due to adjustment of the model from the initial condition. We then begin our simulations of 1997 followed by 1998 for analysis.

3. Results

The model captures the contrasting thermal cycle over the 1997-1998 period. Consistent with observations, 1997 has extreme ice, while 1998 has minimal ice (Figure 3; see Supporting Information movie). Stratification for these years is illustrated in Figure 4, which shows lake-wide average temperature in the upper 50 m layer and a deeper layer, between 150 and 200 m.

For convenience, we define overturning as the time when the average temperatures of the two layers are equal, indicating an isothermal water column, and marks the transition between the winter and summer stratified seasons. As discussed below, this definition is useful to obtain an overall picture of the lake, but it cannot fully capture the spatial heterogeneity.

The warm year, 1998, has a relatively short and weak winter-stratified season (~101 days), which starts in mid-January and lasts until mid-April (Figure 4). The lake's upper 50 m cools to 2.8°C, only 1.2°C colder than the temperature of maximum density. Following this weakly stratified winter, the summer of 1998 is strong. The stratified period lasts ~262 days, and the mean temperature in upper 50 m reaches 9.9°C. In contrast, 1997 has much stronger winter stratification in length and strength (Figure 4). It lasts ~162 days and the temperature difference between the top 50 m and 150-200 m layers reaches 2.4°C. During this period, average surface temperature dips to 1°C. The summer following this strong winter is weak, as the lake-wide upper layer average temperature only reaches 8°C, and the summer stratified period lasts just 219 days.

We note that there is no model drift towards higher temperatures in Figure 4. As noted above, any drift from the initial condition has already been eliminated in the spin-up years. Figure 4 simply shows a cold year followed by a warm year. As previously shown by *White et al.* [2012], interannual variability is well simulated by the model, so the lake cools down to a long term average after the anomalously warm year of 1998.

3.1 Ventilation Age

When the water column is convecting or is very weakly stratified, tracer *Age* everywhere remains close to zero as surface waters are circulated throughout. As stratification sets in, the interior waters begin to age. In March of both 1997 and 1998, when the lake is still experiencing winter stratification, *Age* at 100 m depth shows signs of more significant aging in the western arm (Figure 5a, b; see Supporting Information movie). In contrast, aging is much weaker in areas of complicated bathymetry in the eastern arm (85-86°W). This east-west contrast is observed in both years, but the overall *Age* is younger in 1998 when the winter stratification is weaker and shorter. Cross sections of *Age* at the same time at 47.2° N (Figure 5c, d; see Supporting Information movie) clearly show relatively young ages throughout the entire water column over bathymetric undulations in the eastern arm in both years. In fact, the age of the 200 m deep water near 86°W and adjacent to the rough bathymetry, is significantly younger than the oldest ages in the smoother western arm at much shallower depths.

The time evolution of the *Age* tracer at different water depths shows that aging occurs during periods of strong stratification, which are the summers of both 1997 and 1998 and the cold winter of 1997 (Figure 6). During these times, the rate of aging approaches the maximum rate (i.e., 1 day of aging for 1 simulation day) for waters deeper than 50 m. This indicates a near-complete isolation of these interior waters from the atmosphere. The shallower waters (<50 m, black line, Figure 6) also become older but not nearly as quickly, because zero-age surface water is more easily and continuously mixed into them. Aging occurs to a much greater extent during the longer stratification in the summer than in the winter. This is most prominently seen in 1998, whose summer-stratified period is tens of days longer than in 1997. The maximum *Age* of the lake reaches about 300 days over the entire 1997-1998 period.

Between late summer and early winter (e.g., September to December), *Age* at various depths stops increasing and declines rapidly (Figure 6). This indicates the arrival of the fall overturning; convection of surface waters resets the age of the interior waters. Importantly, there is a lag in how quickly overturning reaches the interior. For example, the *Age* of the shallow waters begins to get reset as early as September, while the *Age* of the deepest waters does not begin to get reset until the end of December. This lag points to the limitation of using the mean temperatures in the two 50 m thick layers at the top and at depth to define the time of overturning (Figure 4). Rather than being a single point in time, overturning occurs over months and is spatially variable. The spring overturning, as seen by the *Age*, is qualitatively similar to the fall overturning.

Figure 6 also shows that the degree to which age is reset during overturning is variable and depends on the strength of the overturning. For example, the mean *Age* between 250 and 350 m (blue line, Figure 6) in June 1997 declines to no less than 125 days before summer stratification sets in and beings to reverse the trend. This indicates that at least going from winter to summer in this icy year, the spring overturning in the model does not ventilate the entire lake. This lack of complete overturning is illustrated even more dramatically when we plot the maximum *Age* of the lake (magenta line, Figure 6).

3.2 Dissolved Oxygen

Given the dependence of O_2 solubility on temperature, the predicted saturation concentration of dissolved O_2 at the surface is high in the winter and low in the summer (black line, Figure 7a). In the model, *in situ* dissolved O_2 (red line) largely tracks the saturation concentration (i.e., high in

winter and low in summer), but there is a lag in time and amplitude. The lag occurs because the gas exchange kinetics is not fast enough to keep up, when the seasonal change in temperature is rapid. In other words, the residence time of surface water is not long enough to reach equilibrium with the atmosphere. For example, at the height of winter, the amount of dissolved O_2 at the surface is less than the saturation concentration. Hence, wintertime surface waters are undersaturated by 25-35 mmol-O_2 m^{-3} averaged over the whole lake; summer surface waters are supersaturated by almost the same amplitude (Figure 7b). We define this difference as the O_2 anomaly ($\Delta[O_2] = [O_2]_{\text{modeled in situ}} - [O_2]_{\text{saturation}}$; note that this is opposite of how AOU is defined). This seasonal pattern of supersaturation and undersaturation, driven by solubility, is well known in the ocean [*Sarmiento and Gruber*, 2006].

However, not all of the $\Delta[O_2]$ seen in Figure 7b is due to solubility changes. There is a contribution from biology, as net primary productivity produces O_2 in the growing season. To assess the biological contribution to changes in $\Delta[O_2]$, we repeated the same model run without biology. The difference between this solubility-only run and the full model run is thus attributed to biology. Under 1997 forcing conditions, we can attribute approximately 10 mmol-O_2 m^{-3}, or 20% of the total $\Delta[O_2]$ change, to primary production.

One of the transitions between lakewide O_2 undersaturation and supersaturation occurs in mid-June, 1997 (Figure 7). Figure 8 shows the spatial pattern of $\Delta[O_2]$ at this time. The surface is supersaturated at the periphery of the lake, because warming starts from the periphery. Consistent with our understanding of the thermal bar, the middle of the lake surface is still winter-like (e.g., <4°C) and therefore it is undersaturated. Enhanced vertical mixing occurring

near the thermal bar would carry the $\Delta[O_2]$ signal into the interior as the thermal bar migrates away from shore.

The annual cycle of dissolved O_2 in the deep lake can be illustrated by the evolution of the $\Delta[O_2]$-*Age* relationship. Figure 9 shows a time series of the lakewide mean $\Delta[O_2]$ vs. *Age* between 150 and 250 m. Beginning in January 1997 (black symbol labeled "1/1/97"), late fall overturning mixes the surface signal of relatively low *Age* and undersaturated $[O_2]$ down to 150-250 m. Through the winter stratified period until June (labeled "1/25/97" to "6/1/97"), these waters remain isolated from the surface, retaining their wintertime $\Delta[O_2]$ signal, while *Age* increases. In the next ~1 month until the beginning of July (labeled "7/5/97"), spring overturning rapidly mixes down more supersaturated (i.e., warm) and young surface waters down to this depth, so that a negative relationship between $\Delta[O_2]$ and *Age* develops for this period of time. Thereafter and through December (labeled "12/15/97"), summer stratification sets in and *Age* increases. At the same time, there is also a modest increase in $\Delta[O_2]$, as any vertical mixing with the overlying water would introduce supersaturated signal, which reflects warmer and more biologically productive waters. A positive relationship thus develops between $\Delta[O_2]$ and *Age* during this period. Then, in ~1 month period from mid-December until January of 1998 (labeled "1/25/98"), deep convective overturning rapidly decreases both *Age* and $\Delta[O_2]$, as young and undersaturated (i.e., cold) surface waters are mixed from above. This completes the annual cycle, and the process is repeated for 1998 (red symbols, Figure 9) but with a shorter winter stratified period and a longer summer stratified period that lasts 230 days (vs. 190 days in 1997) at this water depth.

Note that Figure 9 shows lake wide mean at 150-250 m. If instead any single water parcel were followed, the renewal of the $\Delta[O_2]$ signal during times of overturning would be more abrupt and can occur within days.

4. Discussion

Our model successfully reproduced climatologically contrasting winters with extensive and minimal ice coverage (Figure 3). Our results show that during the relatively weak winter of 1998 as compared to 1997, stratification is weaker (Figure 4), interior *Age* is younger (Figures 5, 6) and vertical *Dye* penetration is stronger (Figure S3). Spring overturning completes early, by the end of April, and consequently the subsequent summer stratified period is longer and thus stronger (Figure 4). The maximum mean *Age* at depth exceeds 300 days at the end of the summer of 1998 (Figure 6).

The icy year of 1997 is the opposite in all respects. For example, interior *Age* is older and *Dye* penetration is weaker in the winter, pointing to stronger stratification (Figure 4). Spring overturning terminates later in June but does not completely ventilate the lake, so the degree to which the deep *Age* is reset is small. During the following weaker and shorter summer, the maximum mean *Age* at depth only reaches 235 days, 35 days younger than in 1998. These model-based ventilation timescales for Lake Superior are consistent with the months-long tritium-helium ages for Lakes Erie, Huron, and Ontario [*Torgersen et al.*, 1977].

This basic contrast in the thermal cycle and the behavior of the *Age* tracer in the warm year versus cold year is a robust feature of the model, because the same contrast is consistently reproduced in the other simulation periods (1985-1987; 2006-2008). For example, the maximum *Age* reaches 250 days in the long stratified summer following a mild winter in 1987; in contrast, the maximum *Age* is nearly 50 days shorter in the shorter summer following a stronger winter in 1985. To first order, the winter ice cover exerts the dominant control over the ventilation of Lake Superior in the model.

There are other robust features of the model, also consistently seen in all simulation periods. For one, there is enhanced vertical mixing during seasonal overturning in areas over rough bathymetry. For example, *Age* is younger and *Dye* concentration is higher in the rougher eastern arm (e.g., 85-86°W) than in the smoother and shallower western arm (e.g., 89.5°W- 91.5°W) for all seasons and years (Figures 5, S3). This suggests that when the water column stratification is weak or nonexistent, momentum from the atmosphere is preferentially frictionally dissipated within the lake by interacting with the bottom. This is well established in the ocean, where the rate of vertical mixing is observed to be high over prominent bathymetric features such as mid-ocean ridges [e.g., *Ledwell et al.*, 2000]. This is also the reason that the global ocean models from the very early days have had enhanced vertical diffusivity in the deeper part of the ocean [*Bryan and Lewis*, 1979]. In ROMS, interior diffusivity due to internal wave breaking [*Gargett and Holloway*, 1984] is combined with shear instability and convective diffusivity to arrive at the total diffusivity. In our model, this enhanced vertical mixing over the rougher eastern basin, shown with the tracers *Age* and *Dye* (Figures 5, S3), is also seen in other tracers such as total inorganic carbon, $\Delta[O_2]$ and temperature (not shown).

Another robust feature of the model is that seasonal overturning takes months to complete. For example, Figure 6 shows that in both 1997 and 1998, fall overturning begins to reset *Age* in September in the top 50 m. Overturning progressively penetrates deeper, until the oldest water is reset in January of the following year. We speculate that in other large lakes, in which seasonal thermal bar is observed, overturning also takes weeks and months to reach the deepest layers, and the process begins at different times in different topographic regimes of the lakes.

The final robust feature we highlight is that the spring overturning does not completely reset the interior *Age*. The maximum *Age* in the model only decreases to 200 days in the spring of both 1997 and 1998 (Figure 6), meaning that some part of the lake did not get ventilated. In general, deep *Age* is reset to a much greater extent in the late fall overturning, which could be due to the stronger winds generating deeper convection, than in the spring overturning.

As noted above, standard chemical oceanography predicts a clear relationship between AOU and *Age*. However, the expected positive relationship is observed in the model only in specific locations during summertime stratification (not shown). One reason is that Lake Superior is both physically dominated and oligotrophic, so that the respiration signal is weak. This biological signal was estimated roughly as a fifth of the total $\Delta[O_2]$. This estimate is likely reasonable, given that the total primary production in the model is comparable to estimates based on observations [*White et al.*, 2012]. Another reason for the lack of persistent $\Delta[O_2]$ -*Age* relationship is that the seasonally oscillating, surface $\Delta[O_2]$ signal (Figure 7b) is transmitted to

the interior during times of overturning (Figure 9). Taken together, the strong and oscillatory physical signal overwhelms the weaker biological signal.

There are a few implications from this study. First, the ventilation age of less than a year implies that Lake Superior should track changes in the atmosphere without much lag. In this regard, the three year lag found in the radiocarbon of Superior's DIC pool relative to the atmosphere [*Zigah et al.*, 2011] is largely consistent. The lag time based on radiocarbon is expected to be somewhat longer anyway, because the transfer of the atmospheric radiocarbon signal to the surface waters requires carbon isotopic equilibration. In the ocean, this takes about ~10 years [*Broecker and Peng*, 1982]. Carbon isotopic equilibration in surface ocean is not actually achieved because the surface water residence time is much shorter than ~10 years, giving the so-called reservoir age. A similar effect is expected in Lake Superior, although it is not clear how large the effect should be, given the large differences in water chemistry. Superior DIC and alkalinity are approximately a third to half of typical oceanic values.

Second, if the real Lake Superior behaves like the model, then most inputs to the lake will get mixed throughout the water column within a year. This may include dry and wet deposition of nutrients and particles from the atmosphere as well as pollutants, which dissolve or are neutrally buoyant and thus drift passively with water. In model results not shown here, *Dye* tracers released at different points around the lake typically take longer to mix horizontally, especially between the western and eastern arms of the lake, than vertically. Therefore a point source input would likely get well mixed vertically within the arm of the lake in which the input occurred,

well before it reaches the deeper levels of the other arm. This is consistent with 2-3 year timescale of horizontal mixing in Superior [*Lam*, 1978].

Is it possible for some part of the lake to remain isolated from the atmosphere for longer than was simulated by our model, perhaps one year or longer? Our results suggest that strong winter stratification followed by strong summer stratification would possibly make that happen. A strong winter seems necessary, because the following spring overturning does not completely reset the deep *Age*. If the following summer were also strong, aging could continue from an incompletely reset *Age* for a longer period of time. Our results indicate that this hypothetical scenario of an unusually strong summer following an unusually icy winter does not seem plausible. The large thermal capacity of the lake gives it a months-long memory, which is not easily erased by surface forcing. Perhaps in the future under a warming planet, high amplitude variability may make the scenario more likely than today. In fact, there is some hint of this in recent studies of polar amplification, which may be leading to more extreme weather events in midlatitudes, as higher amplitude waves in the upper atmosphere propagate more slowly [e.g., *Francis and Vavrus*, 2012].

Acknowledgements

Model development and experiments were funded by the National Science Foundation (NSF-OCE-0825576) and NASA (NNX13AM85G). CG was supported by an NSF-sponsored summer REU internship program at the University of Minnesota (NSF-EAR1062775). Numerical computation was carried out using resources at the University of Minnesota Supercomputing

Institute (MSI). Our numerical model code and model simulation results are archived at MSI and will be made freely available upon request to KM.

Figure captions

Figure 1. Bathymetry of Lake Superior in the model. The three locations where the *Dye* concentration time series are created (Figure S3) are indicated by filled symbols (triangle, circle, and square).

Figure 2. How tracer *Age* works. Vertical mixing reduces *Age* in the interior. See main text for inhibition of *Age* resetting in the presence of ice cover.

Figure 3. Model-simulated maximum surface ice concentration in 1997 ('cold' year) and 1998 ('warm' year). Ice concentration is defined here as areal fraction of grid area covered with ice: 1.0 means 100% covered.

Figure 4. Model-simulated lake-wide mean temperatures in the top 50 m and 150-200 m. Where they intersect indicate times of isothermal conditions and thus overturning.

Figure 5. Model-simulated *Age* in 1997-1998 at 100 m water depth (maps) and along 47.1° N (cross sections). The lines in the maps indicate the location of the sections.

Figure 6. Model-simulated, mean *Age* at different depth layers. "Maximum" refers to the oldest age anywhere in the model domain, typically in the deepest parts of the lake.

Figure 7. Model-simulated surface O_2 cycle. (a) Surface mean dissolved O_2 concentration (red line) and saturation O_2 concentration (black line). (b) Dissolved O_2 concentration minus saturation O_2 concentration.

Figure 8. Model-simulated surface saturation anomaly ($[O_2]_{\text{model in situ}}$-$[O_2]_{\text{saturation}}$) on June 15, 1997. Positive=supersaturation (summer signal); negative=undersaturation (winter signal).

Figure 9. Model-simulated interior O_2 cycle illustrated with saturation anomaly versus *Age* at an average of 200 m. More negative $\Delta[O_2]$ indicates undersaturation (i.e., advection of surface winter signal). Black and red symbols respectively represent calendar years 1997 and 1998.

References

Aeschlback-Hertig, W., R. Kipfer, M. Hofer, D. M. Imboden, and H. Bauer (1996), Density-driven exchange between the basins of Lake Lucerne (Switzerland) traced with the 3H-3He method, *Limnol. Ocean.*, *41*(4), 707–721.

Assel, R. A. (2003), An electronic atlas of Great Lakes ice cover, in *NOAA Great Lakes Ice Atlas*, Great Lakes Environmental Research Laboratory, Ann Arbor, Michigan.

Beletsky, D., J. H. Saylor, and D. J. Schwab (1999), Mean circulation in the Great Lakes, *J. Gt. Lakes Res.*, *25*(1), 78–93.

Bennett, E. B. (1978), Water budgets for Lake Superior and Whitefish Bay, *J. Gt. Lakes Res.*, *4*(3-4), 331–342.

Bennington, V., G. McKinley, and C. H. Wu (2010), General circulation of Lake Superior: Mean, variability, and trends from 1979 to 2006, *J. Geophys. Res.*, *115*(C12015), doi:10.1029/2010JC006261.

Bennington, V., G. McKinley, N. Urban, and C. P. McDonald (2012), Can spatial heterogeneity explain the perceived imbalance in Lake Superior's carbon budget? A model study, *J. Geophys. Res.*, *117*(G03020), doi:10.1029/2011JG001895.

Broecker, W. S., and T.-H. Peng (1982), *Tracers in the Sea*, Eldigio Press, Palisades.

Bryan, K., and L. J. Lewis (1979), A water mass model of the world ocean, *J. Geophys. Res.*, *84*, 2503–2518.

Chen, C. A., and F. Millero (1986), Precise thermodynamic properties for natural waters covering only the limnological range, *Limnol. Oceanogr.*, *31*, 657–662.

Chen, C. S., J. R. Zhu, E. Ralph, S. A. Green, J. W. Budd, and F. Y. Zhang (2001), Prognostic modeling studies of the Keweenaw current in Lake Superior. Part I: Formation and evolution, *J. Phys. Oceanogr.*, *31*(2), 379–395.

Chen, C. S., J. R. Zhu, K. Y. Kang, H. D. Liu, E. Ralph, S. A. Green, and J. W. Budd (2002), Cross-frontal transport along the Keweenaw coast in Lake Superior: a Lagrangian model study, *Dyn. Atmospheres Oceans*, *36*(1-3), 83–102.

Cotner, J. B., B. Biddanda, W. Makino, and E. Stets (2004), Organic carbon biogeochemistry of Lake Superior, *Aquat. Ecosyst. Health Manag.*, *7*(4), 451–464.

England, M. H. (1995), The age of water and ventilation timescales in a global ocean model, *J. Phys. Oceanogr.*, *25*(11), 2756–2777.

Fasham, M. J. R., H. W. Ducklow, and S. M. McKelvie (1990), A nitrogen-based model of plankton dynamics in the oceanic mixed layer, *J. Mar. Res.*, *48*(3), 591–639.

Fer, I., U. Lemmin, and S. A. Thorpe (2002), Winter cascading of cold water in Lake Geneva, *J. Geophys. Res.*, *106*(C6), 3060, doi:10.1029/2001JC000828.

Forel, F. A. (1880), La conglation des lacs Suisses et savoyards pendant l'hiver 1879-1880, *11 - Lac Leman Echo Alpes*, *3*, 149–161.

Francis, J. A., and S. J. Vavrus (2012), Evidence linking Arctic amplification to extreme weather in mid-latitudes, *Geophys. Res. Lett.*, *39*(L06801), doi:10.1029/2012GL051000.

Gargett, A. E., and G. Holloway (1984), Dissipation and diffusion by internal wave breaking, *J. Mar. Res.*, *42*(1), 15–27.

Harrington, M. W. (1895), *Surface currents of the Great Lakes*, Bulletin, Weather Bureau, U.S. Department of Agriculture, Washington D.C.

Hecky, R. E. (2000), A biogeochemical comparison of Lakes Superior and Malawi and the limnological consequences of an endless summer, *Aquat. Ecosyst. Health Manag.*, *3*, 23–33.

Hofer, M., F. Peeters, W. Aeschlback-Hertig, M. Brennwald, J. Holocher, D. M. Livingston, V. Romanovski, and R. Kipfer (2002), Rapid deep-water renewal in Lake Issyk-Kul (Kyrgyzstan) indicated by transient tracers, *Limnol. Ocean.*, *47*(4), 1210–1216.

Hohmann, R., R. Kipfer, F. Peeters, G. Piepke, and D. M. Imboden (1997), Processes of deep-water renewal in Lake Baikal, *Limnol. Ocean.*, *42*(5), 841–855.

Hohmann, R., M. Hofer, R. Kipfer, F. Peeters, and D. M. Imboden (1998), Distribution of helium and tritium in Lake Baikal, *J. Geogr. Res.*, *103*(C6), 12823–12838.

Hubbard, D. W., and J. D. Spain (1973), The structure of the early spring thermal bar in Lake Superior, in *Proceedings of the 16th Conference on Great Lakes Research*, pp. 735–742.

Lam, D. C. L. (1978), Simulation of water circulation and chloride transports in Lake Superior from summer 1973, *J. Gre*, *4*(3-4), 343–349.

Ledwell, J. R., E. T. Montgomery, K. L. Polzin, L. C. St. Laurent, R. W. Schmitt, and J. Toole (2000), Evidence for enhanced mixing over rough topography in the abyssal ocean, *Nature*, *403*, 179–182.

Matheson, D. H., and M. Munawar (1978), Lake Superior basin and development, *J. Gt. Lakes Res.*, *4*(3-4), 249–263.

Matsumoto, K. (2007), Radiocarbon-based circulation of the world oceans, *J. Geophys. Res.*, *112*(C09004), doi:10.1029/2007JC004095.

McKinney, P., B. Holt, and K. Matsumoto (2012), Small eddies observed in Lake Superior using SAR and sea surface temperature data, *J. Gt. Lakes Res.*, *accepted*.

McManus, J., E. A. Heinen, and M. M. Baehr (2003), Hypolimnetic oxidation rates in Lake Superior: Role of dissolved organic material on the lake's carbon budget, *Limnol. Oceanogr.*, *48*(4), 1624–1632.

Messias, M.-J., C. Andrie, L. Memery, and H. Mercier (1999), Tracing the North Atlantic Deep Water through the Romanche and Chain fracture zones with chloroflouromethants, *Deep Sea Res.*, *46*, 1247–1278.

Peeters, F., D. Finger, M. Hofer, M. Brennwald, D. M. Livingstone, and R. Kipfer (2003), Deep-water renewal in Lake Issyk-Kul driven by differential cooling, *Limnol. Ocean.*, *48*(4), 1419–1431.

Rhein, M., L. Stramma, and G. Krahmann (1998), The spreading of Antarctic Bottom Water in the tropical Atlantic, *Deep Sea Res.*, *45*, 507–527.

Russ, M. E., N. E. Ostrom, H. Gandhi, P. H. Ostrom, and N. R. Urban (2004), Temporal and spatial variations in R : P ratios in Lake Superior, an oligotrophic freshwater environment, *J. Geophys. Res.-Oceans*, *109*(C10).

Sarmiento, J. L., and N. Gruber (2006), *Ocean Biogeochemical Dynamics*, Princeton University Press, Princeton.

Schlitzer, R. (1986), 14C in the deep water of the eastern Atlantic, *Radiocarbon*, *28*(2A), 391–396.

Schmidt, M., N. M. Budnev, N. G. Granin, M. Sturm, M. Schurter, and A. Wuest (2008), Lake Baikal deepwater renewal mystery solved, *Geophys. Res. Lett.*, *35*(L09605), doi:10.1029/2008GL033223.

Shchepetkin, A. F., and J. C. McWilliams (2005), The regional ocean modeling system (ROMS): A split-explicit, free surface, topography-following coordinate ocean model, *Ocean Model.*, *9*, 347–404.

Shimaraev, M. N., N. G. Granin, and A. A. Zhdanov (1993), Deep ventilation of Lake Baikal waters due to spring thermal bars, *Limnol. Ocean.*, *38*(5), 1068–1072.

Small, G. E., J. B. Cotner, J. C. Finlay, R. A. Stark, and R. W. Sterner (2014), Nitrogen transformations at the sediment–water interface across redox gradients in the Laurentian Great Lakes, *Hydrobiolgia*, *731*(doi:10.1007/s10750-013-1569-7).

Sterner, R.W. (2010), In situ-measured primary production in Lake Superior, *J. Gt. Lakes Res.*, *36*, 139–149.

Torgersen, T., Z. Top, B. Clarke, W. J. Jenkins, and W. S. Broecker (1977), A new method for physical limnology-tritium-helium 3 ages-results for Lakes Erie, Huron, and Ontario, *Limnol. Ocean.*, *22*(2), 181–193.

Ullman, D., J. Brown, P. Conillon, and T. Mavor (1998), Surface temperature fronts in the Great Lakes, *J. Gt. Lakes Res.*, *24*(4), 753–775.

Urban, N. R., M. T. Auer, S. A. Green, X. Lu, D. S. Apul, K. D. Powell, and L. Bub (2005), Carbon cycling in Lake Superior, *J. Geophys. Res.-Oceans*, *110*(C6).

Weiss, R. F., E. C. Carmack, and V. M. Koropalov (1991), Deep-water renewal and biological production in Lake Baikal, *Nature*, *349*, 665–669.

White, B., and K. Matsumoto (2012), Causal mechanisms of the deep chlorophyll maximum in Lake Superior: A numerical modeling investigation, *J. Gt. Lakes Res.*, *38*, 504–513.

White, B., J. Austin, and K. Matsumoto (2012), A three dimensional model of Lake Superior with ice and biogeochemistry, *J. Gt. Lakes Res.*, *38*, 61–71.

Zigah, P. K., E. C. Minor, J. P. Werne, and S. L. McCallister (2011), Radiocarbon and stable carbon isotopic insights into provenance and cycling of carbon in Lake Superior, *Limnol. Oceanogr.*, *56*(3), 867–886.

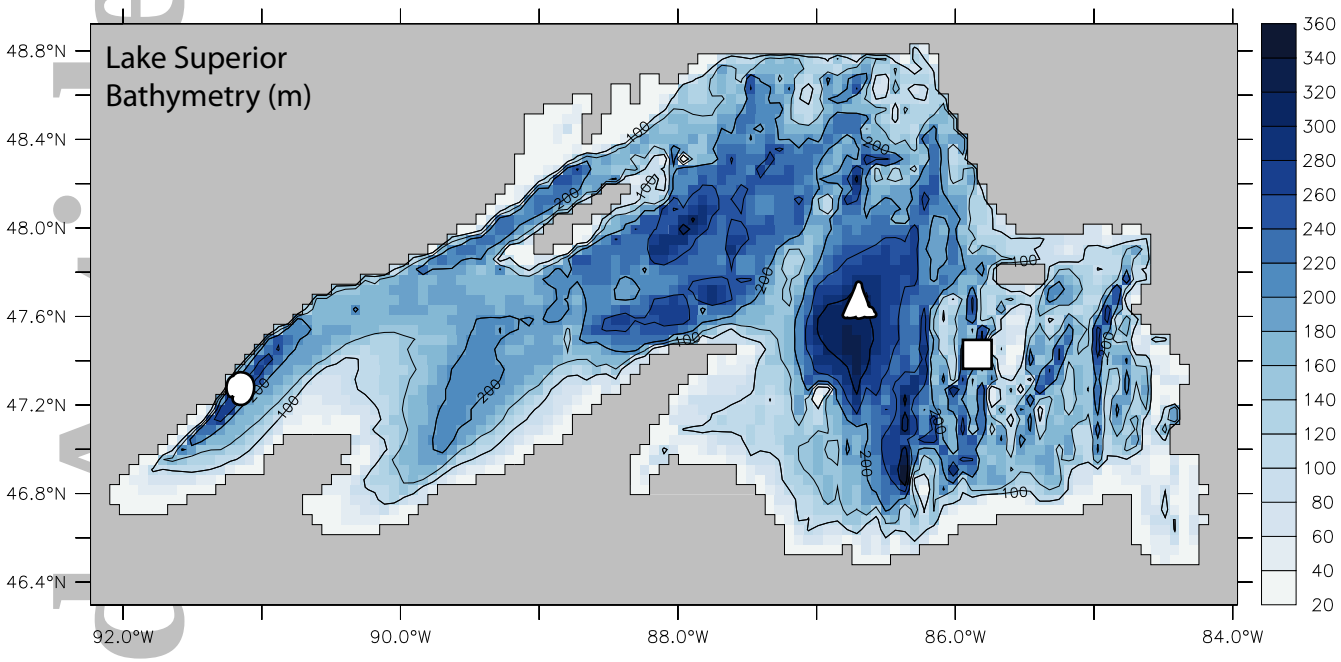

a) $t_0 = 0$

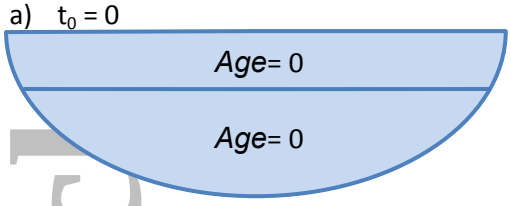

b) $t_1 = t_0 + \Delta t$

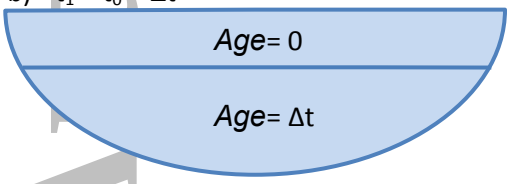

c) $t_2 = t_1 + \Delta t$